Research Article | Vol. 29, No. 2 / 18 January 2021 / Optics Express 1232

Optics EXPRESS

Advanced volume holographic filter to improve the SNR of polychromatic sources in a noisy environment

PEDRO ENRIQUE ALCARAZ AND PIERRE-ALEXANDRE BLANCHE*

Wyant College of Optical Sciences, University of Arizona, 1630 E University Blvd., Tucson, AZ 85721, USA
**pablanche@optics.arizona.edu*

Abstract: We present a new type of filter that improves the SNR of systems where polychromatic signal and noise are located at different distances within the same line of sight. The filter is based on holographic technology that allows for the discrimination of wavefronts by range. In using a combination of two holographic elements, a pre-disperser and a thick volume hologram, we were able to significantly increase the spectral bandwidth of the filter, from 9nm without the pre-disperser to 70nm with both holographic elements. Laboratory proof of concept demonstrated that such a filter is capable of an SNR improvement of 15 dB for a monochromatic source, and up to 7.6 dB for a polychromatic source. This filter can find applications in astronomic observation, satellite or space debris tracking, and free-space optical communication.

1. Introduction

Ground-based detection and tracking of artificial satellites have been of great public and private interest ever since the launch of Sputnik in 1957 [1,2]. Since then, many advances in hardware and software have allowed for nighttime custody of satellites; however, full 24hr custody has remained a challenge primarily due to the low signal to noise ratio (SNR) during daylight hours. Most daytime background noise comes from Rayleigh-scattered sunlight, originating 30 km above sea level [3]. This particular form of noise has been difficult to deal with primarily because of its variable nature; where, the total brightness, spectra, and polarization state of Rayleigh-scattered light is dependent on the atmospheric transparency, altitude, meteorological conditions, and location of the sun during imaging [4–6].

Prior approaches have leveraged the spectral differences between satellites (red) and the sky (blue), using long focal length telescopes and carefully managed camera saturation, to increase the retrieval daytime imaging SNR [1]. Researchers also introduced near-infrared (NIR) [7–9], and shortwave infrared (SWIR) sensors in an attempt to track low Earth orbiting (LEO) and geosynchronous equatorial orbit (GEO) satellites [9–11]. Nevertheless, state-of-the-art imaging systems still suffer from low SNRs and have very narrow spectral bandwidths, substantiating the need for improved imaging modalities to make the technology more effective and accessible.

Recently, researchers have proposed the use of volume holograms as optical filtering elements (VHF) for ground-based detection and tracking of artificial satellites [12]. By utilizing the Bragg condition, depth-based wavefront selection is made possible. Previously, VHF elements had been used to measure and filter noise in light scattering media based on angular/wavelength dependent selectivity [13,14]. These same properties have been used range based wavefront selection, allowing one to passively select for wavefronts originating from 160-30,000 km, LEO and GEO respectively, while discarding all other wavefronts, i.e. Rayleigh-scattered sunlight at 30 km. Sinha et al., (2002), and subsequently Goa at al., (2013), as well as Chen et al., (2014) utilized a VHF coupled to a telescope objective, referred to as the Volume Hologram Telescope (VHT) arrangement, to increase the resolvable SNR of polychromatic sources who's wavefronts are subject to medium induced scattering effects (i.e. satellite imaging) [12,15,16]. Chen et al.,

#414217 https://doi.org/10.1364/OE.414217
Journal © 2021 Received 9 Nov 2020; revised 18 Dec 2020; accepted 18 Dec 2020; published 6 Jan 2021

Optics EXPRESS

(2014) reported a 6.3 dB SNR improvement for polychromatic point sources (located 5m away) with polychromatic noise (located 1m away) under laboratory conditions. However, a major drawback to using the VHT technique alone lies in the stringent spectral selectivity enforced by the VHF's Bragg condition. Where, in imaging a polychromatic point source, such as an LEO/GEO satellite, the VHF technique can only resolve a 9nm spectral bandwidth, leading to a major loss in retrievable spectral information.

A variety of approaches can be taken to increase the spectral bandwidth of the proposed VHT arrangement. One approach would be to use multiplexed and wavelength-coded holographic gratings to simultaneously obtain information from a specific depth at a variety of colors [17,18]. However, these methods are limited to the holographic material properties, where materials with a large dynamic range, $M_{\#}$, are necessary in order to record multiplexed holograms, thus limiting the number of wavelengths encoded [19]. Furthermore, being that the diffraction efficiency of each hologram is inversely proportional to the square of the number of holograms recorded, the diffraction efficiencies at each wavelength would vary significantly [20]. These factors motivate the need for a different approach for efforts who's aim is to substantially increase the spectral bandwidth of VH based imaging.

Here we propose the Advanced Volume Holographic Filter (AVHF), an optical system consisting of two coupled holographic elements, with aims to increase the spectral bandwidth capabilities of the current volume hologram based filtering approaches while maintaining range-based signal selectivity. Briefly, the AVHF is composed of a thin-volume hologram functioning as a pre-disperser (PD) used to Bragg match the spectra of an incoming wavefront to a thick-volume hologram (VHF) capable of depth-based wavefront selection. Our laboratory proof of concept demonstrated a resolvable spectral bandwidth increase from 8-9nm to 35-70nm when moving from single VHF imaging arrangements to the AVHF arrangements. Furthermore, the range-based signal selectivity of the VHF imaging arrangement was improved by ~2-3 dB when using the proposed AVHF arrangement.

2. Theoretical basis

2.1. Holograms

According to the Klein and Cook criteria [21], the diffracting behavior of volume holograms can be characterized by the "Q" parameter, defined via Eq. (1). VHs are considered thick if $Q \geq 10$, and exhibit Bragg-like diffraction; otherwise, VHs are considered thin if $Q < 1$, operating in the Raman-Nath regime.

$$Q = \frac{2\pi\lambda_R L}{n_0 \Lambda^2 cos\theta} \tag{1}$$

Here, λ_R refers to the VH recording wavelength, n_0 is the material's index, Λ is the holograms grating density, L is the thickness of the hologram, and θ the angle of incidence.

Thick VHs allow for multiple light/matter interactions within medium, making the hologram sensitive to both reading angle and wavelength [22]. For VH gratings with sinusoidal index modulations, Kogelnik's coupled-wave analysis can be used to determine the VH's theoretical diffraction efficiency see Eq. (2) [23].

$$\eta_B = sin^2\left(\frac{\pi\Delta n L}{\lambda cos\theta_B}\right) \tag{2}$$

Where, Δn is the index modulation of the phase pattern, λ is the wavelength of the incident light, L is the thickness of the hologram, and θ_B is the Bragg angle. Note that outside the Bragg

Optics EXPRESS

condition, the holographic grating still diffracts some energy, described via Eqs. (3)–(4).

$$\eta(\theta_i) = \frac{sin^2(\sqrt{\Delta\theta_i}\frac{\pi\Delta nL}{\lambda cos\theta_i})}{\Delta\theta_i} \tag{3}$$

$$\Delta\theta_i = 1 + (\frac{2nsin\theta_B(sin\theta_i - sin\theta_B)}{\Delta n})^2 \tag{4}$$

The VH Bragg condition has recently been exploited in imaging systems to discriminate between wavefronts by range. Examples of volume holographic imaging systems include the development of a 2D scanning confocal microscope [24], as well as a pseudo-3D endoscope capable of passively imaging multiple tissue depths (40-50μm apart) simultaneously [25,26].

2.2. Angular and spectral selectivity

The performance of a VHF for depth based wave front selection is largely dependent on the angular selectivity of the VH element. Recording thick VHF with high Q parameters >> 10 result in highly selective filters; however by increasing the effective length of a VH the diffracted spectral bandwidth of the system is significantly reduced. To mitigate this issue, we devised the Advanced Volume Holographic Filter (AVHF). The AVHF is composed of two coupled holographic elements namely: a thin volume hologram, referred to as a pre-disperser (PD) and a thick hologram, refereed to as a volume hologram filter (VHF).

The AVHF makes use of a PD element to modify the propagation vectors of wavelengths outside the nominal recording wavelength λ_R. The aim of the PD is to Bragg match the entire spectral bandwidth of an incoming wavefront onto a VHF. To motivate this phenomena consider the properties of a thick holographic element recorded at and angle θ_R with a recording wavelength λ_R. The line density, Λ, of the hologram is fixed and can be resolved via Eq. (5), where Λ has units of lines-pairs per millimeter (lp/mm).

$$\Lambda = \frac{2sin\theta_{R/2}}{\lambda_R} \tag{5}$$

Under the recording conditions, λ_R and θ_R, the Bragg diffraction angle can be derived, where θ_B is dependent on both λ_R and Λ, see Eq. (6).

$$\sin\theta_B = m\frac{\lambda_R}{2\Lambda}; m \in \mathbb{N} \tag{6}$$

Combining Eqs. (5)–(6) a wavelength-dependent diffraction angle is given via Eq. (7).

$$\theta_B(\lambda) = \arcsin[\frac{\lambda}{\lambda_R}(sin\frac{\theta_R}{2})] \tag{7}$$

Taking Eqs. (3) and (7) into consideration, wavelengths outside the recording wave λ_R can be diffracted through a thick VH so long as their angle of incidence coincide with $\theta_B(\lambda)$, this property is commonly referred to as the blaze curve of the a VH.

A wavelength dependent modification to the propagation vectors of an incoming wavefront is achievable via the introduction a thin holographic element, PD, operating near or at Q = 10, see Fig. 1. The PD diffracted wavefront will feature a wavefront with modified propagation vectors $\mathbf{k}_{p,\lambda}$, each of which will be Bragg matched onto the VHF so long as the PD is recorded with the same recording parameters as used in the VHF, this property is commonly referred to as the super blaze curve and corresponds to the envelope of the blaze-curves from the VH.

Figure 2 provides an example of the phenomena discussed. Figure 2(a) considers a thick VHF with a grating density Λ = 2659 lp/mm and recording wavelength λ_R = 532nm. The Bragg angle

Optics EXPRESS

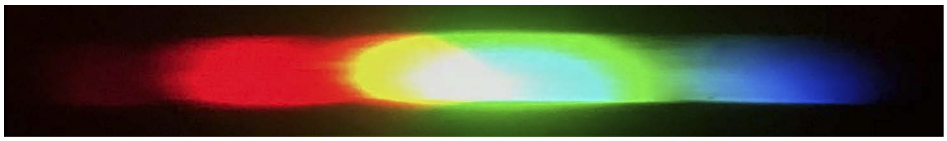

Fig. 1. Polychromatic wavefront diffracted by an 16μm PD element recorded at $\lambda_R = 532$nm and $\theta_R = 90°$.

of such the VHF would be $\theta_B(532nm) = 45°$. Here, an overview of wavelength-dependent Bragg diffraction is provided; where, at three wavelengths $\lambda = 465nm, 532nm$, and $655nm$, diffraction is only possible if the incident propagation vectors, $\mathbf{k}_{p,\lambda}$, meet the Bragg criterion. Note that the Bragg criterion can be met for wavelengths outside the recording wavelength λ_R so long as the incidence angle coincides with $\theta_B(\lambda)$. Figure 2(b) considers the AVHF consisting of a 16 μm PD coupled to a 2mm thick VHF, both with grating densities $\Lambda = 2659$ lp/mm and recording

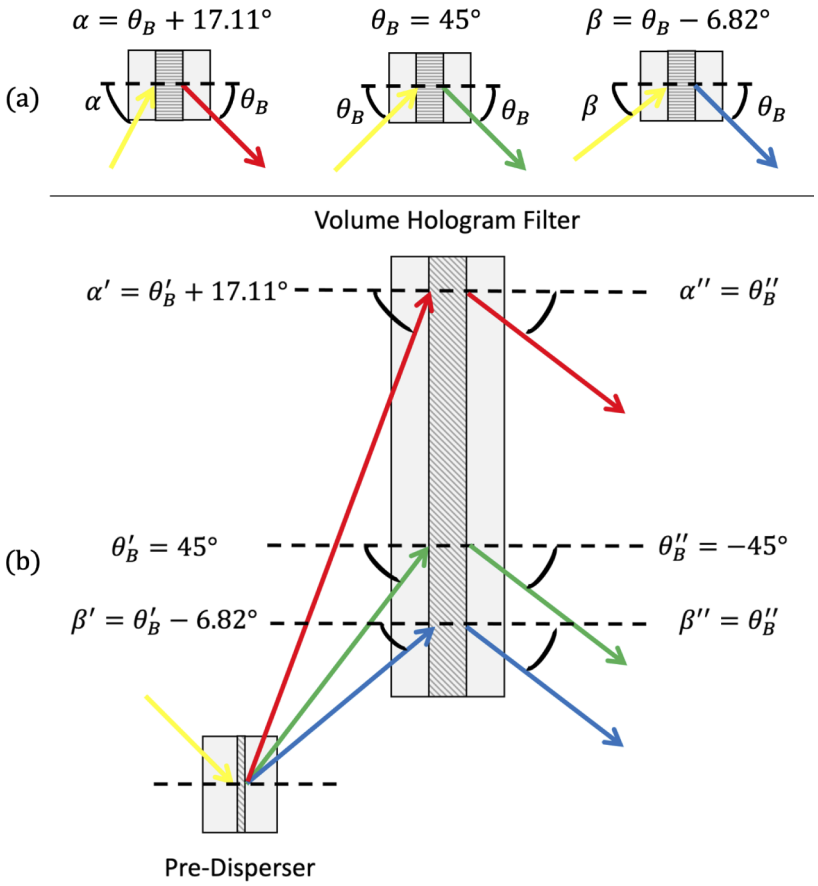

Fig. 2. (a) Schematic demonstrating wavelength-dependent Bragg diffraction in a thick-volume hologram. The angle α pertains to the wavelength-dependent Bragg angle, $\theta_B(665nm)$, required for diffraction at $\lambda = 665$nm, similarly $\beta = \theta_B(465nm)$. (b) Schematic demonstrating the AVHF system, where an incident polychromatic collimated wavefront (yellow arrow) is Bragg matched via the PD element to the VHF. Arrow colors are indicative of wavelength, where red is λ=665nm, green is λ=532nm, and blue is λ=465nm.

Optics EXPRESS

wavelength λ_R = 532nm. Here the PD diffracted propagation vectors meet the Bragg criterion of the VHF; where angles $\alpha^{'}, \beta^{'}, \theta_B^{'}$ and $\alpha^{''}, \beta^{''}, \theta_B^{''}$ correspond PD and VHF diffracted wavelengths $\lambda = 465nm, 532nm$, and $655nm$ respectively.

Theoretically, by introducing a PD to Bragg match the wavelength-dependent angles of incidence onto the VHF, the spectral bandwidth of the system can be as large as the convolution between the blaze of the PD and the super-blaze of the VHF, which is several orders of magnitude larger than with the VHF alone. Considering Kogelnik's Coupled Wave Theory, when a $4\mu m$ PD is coupled to the 2 mm VHF the spectral bandwidth (FWHM) of the system becomes 80 nm, ~500x times larger than without the PD; where the 2 mm VH would have a spectral bandwidth of ~0.15 nm.

3. Methods

We demonstrated the advantage of the AVHF configuration in a laboratory setup. PD elements were recorded in a commercial photopolymer (Bayfol HX200), the VHF element was made of a thick PQ-doped PMMA material. Monochromatic and polychromatic light sources were used to produce wavefronts simulating far off objects. Atmospheric noise was simulated by passing the monochromatic and polychromatic wavefronts through a diffuser located in front of the AVHF system.

3.1. Hologram recording arrangement

The holograms were recorded using an Nd:YAG laser with center wavelength at λ_R = 532nm. Both the signal and reference arms were collimated and incident to the holographic recording material in a symmetric configuration, i.e. when recorded at θ_R, the signal beam is incident on the VH at $-\frac{\theta_R}{2}$ and the reference, beam is incident on the VH at $\frac{\theta_R}{2}$.

3.2. Materials for volume holograms

The materials used to record the PD element were the Bayfol HX200 photopolymer with thicknesses of 4μm and 16μm. The exposure energy required for the Bayfol HX thin-volume holograms where 25 mJ/cm^2, after that the samples were exposed to an incoherent halogen white light source for ~5 min to fix the recorded index modulation.

Considering the lack of commercially available material for very thick (>1mm) holograms, we opted to synthesize phenanthrenequinone- doped poly-(methyl-methacrylate), (PQ-doped PMMA). PQ-doped PMMA is a photosensitive polymer that displays minimal shrinkage and deviation from recorded index modulation making it attractive for holographic applications; furthermore, the material can be cast in a mold, allowing for material thicknesses >1mm [19,27].

The exposure energy required for the thick-volume holograms where 600 J/cm^2. As a post-exposure treatment, the PQ-doped PMMA holograms were placed in a dark container for 24hrs, allowing for unexposed PQ diffusion. Thereafter, the hologram was exposed to an incoherent halogen white light source for 24hrs. Indeed, studies have found that grating strength can be increased by allowing unexposed PQ molecules to diffuse into exposed regions, generating a homogeneous post-exposure PQ concentration across the sample [20,28].

3.3. Hologram characterization

3.3.1. Angular selectivity and diffraction efficiency

The measurements of angular selectivity and diffraction efficiency were carried out by exposing the PD and VHF to a collimated beam from an Nd:YAG laser with center wavelength at λ = 532nm. The holograms were mounted on a manual rotation stage; measurements were taken at $\theta_B \pm \Delta\theta$. The zero, first order, and second-order (when applicable) diffracted beam intensities were measured using a Newport Optical Power Meter Model No. 1917-R.

Optics EXPRESS

3.3.2. Wavelength selectivity

The measurements of wavelength selectivity were carried out by exposing the PD and VHF to a collimated beam from an NKT SuperK COMPACT supercontinuum laser. The holograms were mounted on a manual rotation stage; spectral measurements were taken at the zero and first order diffracted beams using an OceanOptics USB4000 fiber spectrometer.

Since the first-order diffraction is spectrally disperse, the light was focused onto a 5° diffuser and then coupled with a second lens onto the spectrometer input fiber. This procedure was used to avoid wavelength dependent coupling losses and allowed for repeatable measurements.

3.4. Design of the AVHF-telescope

A tabletop arrangement was set up to synthetically generate monochromatic and polychromatic wavefronts. In an effort to emulate conditions similar to those present in daylight satellite imaging, the source and noise distances were scaled down to accommodate the laboratory space. Similar arrangement was use successfully in Goa at al., (2013), and subsequent work to demonstrate the principle of the holographic filter. Source and noise synthetic wavefronts with curvature were generated using a monochromatic and a polychromatic source [15,16]. Wavefront curvature was generated by focusing the mono/polychromatic beams 13m out using a telephoto objective (L1). Both monochromatic and polychromatic noise at short distance was introduced to the system by scattering the synthetically generated wavefronts with a 5° diffuser. Note that although diffuse noise may not be entirely representative of atmospheric scattering (wavelength dependency, thickness distribution, and coherence), it serves as a good indicator of how the system will perform under those conditions. Additionally, the same type of noise was introduce in Goa at al., (2013), and subsequent work, which helps for the comparison between systems [15,16].

A telescope arrangement, comprised of a 2x microscope objective and a bi-convex lens, L2, with a focal length of 75mm, was used to generate a magnified and collimated beam incident on the VHF and AVHF holographic systems respectively, see Fig. 3.

A Nd:YAG laser with center wavelength at λ = 532nm, and a NKT SuperK COMPACT supercontinuum laser were used as light sources. The Nd:YAG laser was used to align the entire system and measure the SNR of the synthetic monochromatic source and noise. The NKT SuperK COMPACT supercontinuum laser was used to measure the SNR for a polychromatic source and noise.

3.5. SNR measurements

SNR measurements were made using the tabletop setups presented in Figs. 3(a)-(c). A UI-1220SE, 752x480, 0.36 mega-pixel camera with a color WVGA sensor was utilized to measure the intensity of the incoming light. The gain, exposure, and frame-rates were adjusted to accommodate for the noise measurements and thereafter fixed for subsequent signal measurements. To make sure no detector non-linearity was introduced to the measurements, the signal was measured with the same camera parameters (gain, exposure, and frame-rate) as used when measuring system noise and an appropriate ND filter was placed in front of the camera to avoid saturation.

The signal and noise measurements were taken separately. Noise measurements were made by placing a 5° diffuser in front of the telescope. The signal measurements were made without the 5° diffuser. The average ratio of signal to noise was calculated using power SNR:

$$SNR = 10\log_{10}\left(\frac{P_{signal}}{P_{noise}}\right) \tag{8}$$

Optics EXPRESS

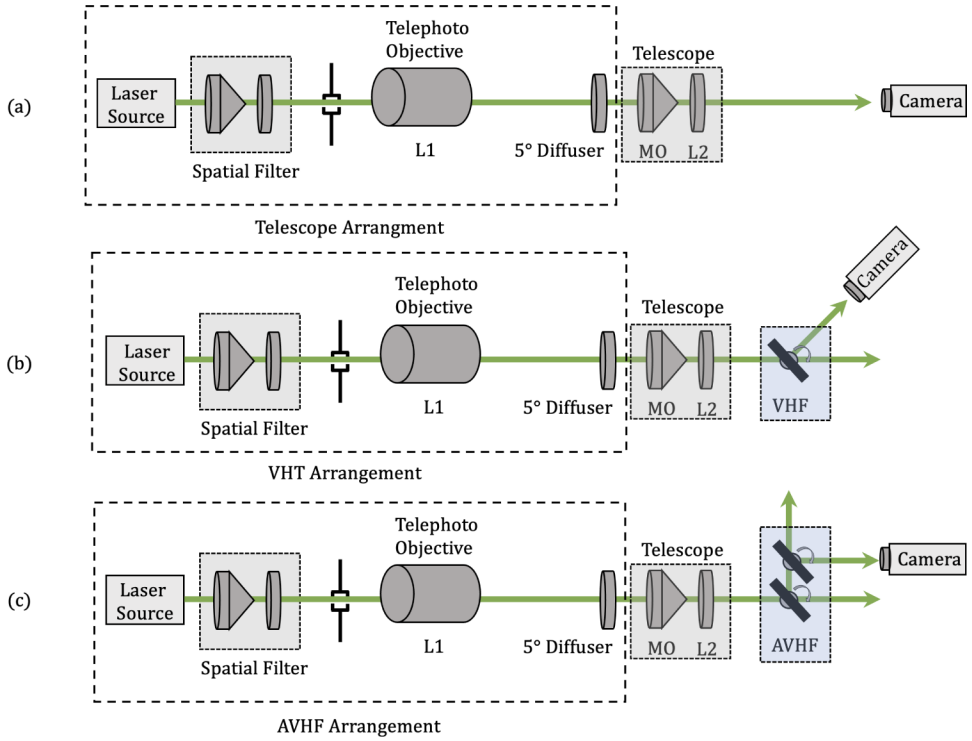

Fig. 3. Schematic of the synthetic source/noise imaging arrangements. (a) features imaging via a telescope, (b) imaging via a telescope coupled to a VHF element, and (c) imaging via a telescope coupled to the AVHF system.

4. Results and discussion

4.1. Characterization of materials

Two AVHF, working at $\theta_R = 90°$ and $\theta_R = 20°$, were examined in this work. Both, the PD and VHF elements of the AVHFs were characterized after the recording process. Angular and spectral selectivity measurements were fitted to Kogelnik's coupled-wave analysis to retrieve the index modulation, Δn, and the recorded effective hologram thickness, L_{eff}.

4.1.1. Angular/spectral selectivity and diffraction efficiency

Angular and spectral selectivity measurements for the individual AVHF elements at $\theta_R = 90°$ were fitted to expected values obtained via Kogelnik's Coupled Wave Analysis. Figures 4(a) and (b) demonstrate the angular and spectral bandwidth measurements of 16 μm Bayfol. Figures 4(c) and (d) demonstrate the angular and spectral bandwidth measurements of 2.3 mm PQ-doped PMMA. By fitting the data to Kogelnik's Coupled Wave Analysis effective index modulations of $\Delta n = [0.024, 12 \times 10^{-5}]$ and thicknesses of $L_{\text{eff}} = [11.5\mu m, 500\mu m]$ were achieved for the PD and VHF respectively. Results concur with the theoretical expected angular and spectral bandwidths; however, Fig. 4(d), corresponding to the VHF element, had a significantly larger spectral bandwidth than expected (10 nm instead of 2 nm). This may suggests that recording at very high fringe densities, Λ = 2659 lp/mm, did not produce holograms with reliable sinusoidal index modulation throughout the entirety of the recorded volume. We believe that the recording setup was not stable enough to maintain a 367nm grating spacing throughout the recording process and the experiment would benefit from a phase-stabilized recording.

Optics EXPRESS

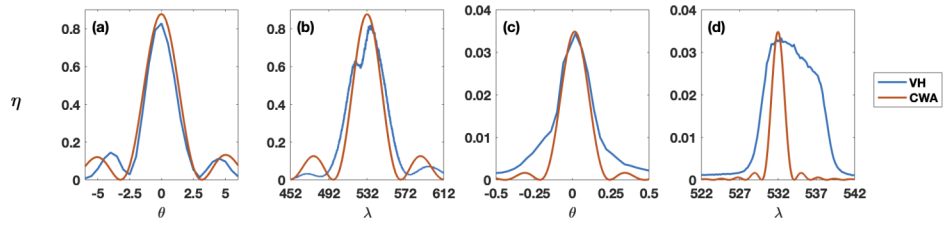

Fig. 4. Angular and spectral bandwidth measurements of (a-b) 16 μm Bayfol and (c-d) 2.3mm PQ-doped PMMA, both recorded at $\theta_R = 90°$, compared to theoretical values obtained via coupled wave analysis via Eq. (3).

The angular and spectral selectivity measurements for the elements of a second AVHF system, recorded at $\theta_R = 20°$, were fitted to expected values obtained via Kogelnik's Coupled Wave Analysis. Figures 5(a) and (b) demonstrate the angular and spectral bandwidth measurements of 4 μm Bayfol. Figures 5(c) and (d) demonstrate the angular and spectral bandwidth measurements of 2.87mm PQ-doped PMMA. The effective index modulations of $\Delta n = [0.021, 12 \times 10^{-5}]$ and thicknesses of $L_{\text{eff}} = [3.5\mu m, 550\mu m]$ were achieved for the PD and VHF respectively. Results also concur with the theoretical expected angular and spectral bandwidths; however, Fig. 5(b), corresponding to the PD element shows an experimental spectrum that has more structure than the smooth curve predicted for the PD. We believe this is a consequence of the material absorption and the Fresnel reflection by the Bayfol thin film.

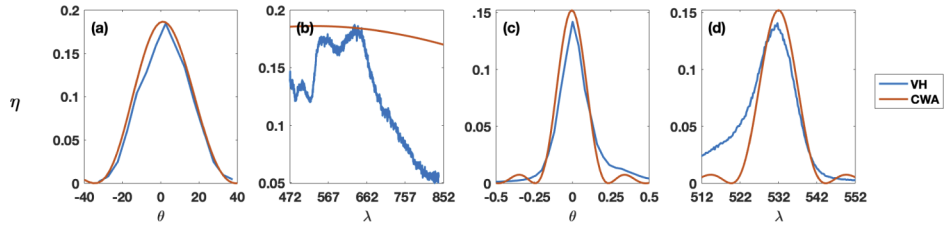

Fig. 5. Angular and spectral bandwidth measurements of (a-b) 4 μm Bayfol and (c-d) 2.87mm PQ-doped PMMA, both recorded at $\theta_R = 20°$, compared to theoretical values obtained via coupled wave analysis.

Note that the refractive index modulations for both the PDs and the VHFs coincide closely with previously reported index modulations achieved in PQ-doped PMMA volume holograms, $\Delta n = [10 \times 10^{-5}, 30 \times 10^{-5}]$, and the expected index modulations prescribed in the Bayfol HX200 data sheet, $\Delta n = 0.03$ [29,30]. However, in the effective thicknesses of the VHF deviated from the actual material thickness. We believe the discrepancy between the VHF hologram thickness and the effective recorded thickness can be attributed to the exposure energy, where 600 J/cm^2 may not have been enough energy to expose the entire length of the PQ-doped PMMA material, leading to low VHF diffraction efficiencies.

4.1.2. PD to VHF Bragg matching efficiency

Spectral measurements were made to determine the spectral bandwidth incident upon each element in both the VHT and AVHF systems. Through these measurements we were also able to quantify the PD to VHF coupling efficiency in the AVHF arrangement. The spectra diffracted by each optical element are shown in Fig. 6.

It is immediately apparent from Figs. 6(a) and (b) that the spectra diffracted by the AVHFs (yellow) has a much broader than the spectrua diffracted by the VHF alone (purple). This

Optics EXPRESS

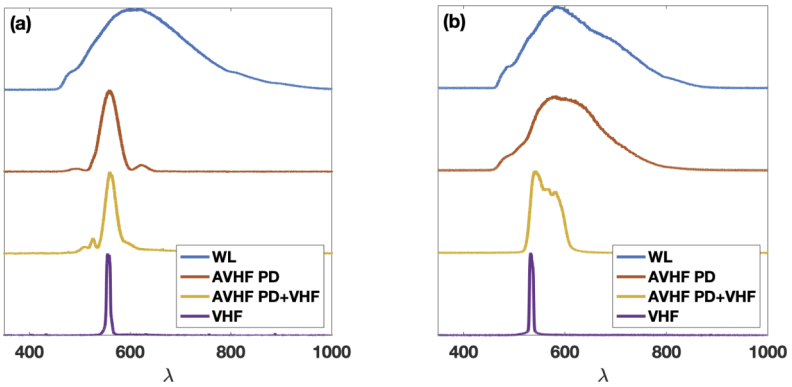

Fig. 6. (a) BLUE spectra pertaining to white light incident on 16μm, $\theta_R = 90°$ PD, RED spectra diffracted by the PD and incident on the 2.3mm, $\theta_R = 90°$, VHF, YELLOW spectra diffracted by the VHF, PURPLE white light diffracted by the 2.3mm, $\theta_R = 90°$, VHF element alone (uncoupled). (b) Similar spectra to those appearing in (a) with a 4μm $\theta_R = 20°$ PD element and 2.87mm, $\theta_R = 20°$, VHF element.

demonstrates unequivocally that the introduction of the PD element is effective in increasing the spectral bandwidth of the VHF element.

The spectral measurements presented in Figs. 6(a) and (b) are summarized in Table 1. Where it can be appreciated that the PD element in the AVHF configuration increases the resolvable spectral bandwidth of the 20° VHF by a factor of 8.75x, and a factor of 3.88x for the 90° VHF. Not quite as large as the theoretical prediction, but significant nonetheless. See Fig. 7 for a visual representation of the increase in spectral bandwidth.

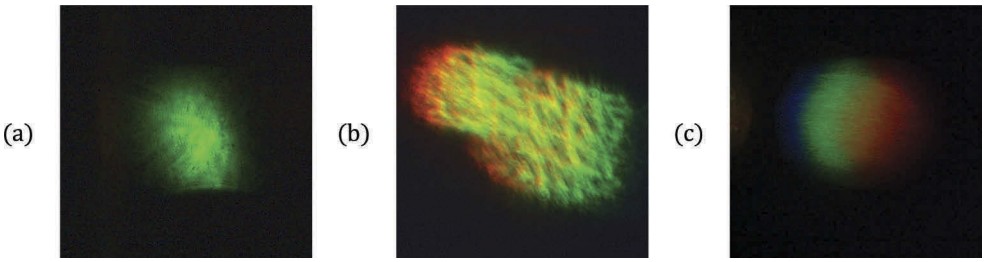

Fig. 7. Images collected in the SNR measurement process. Images (a-b) are pictures of the diffracted signal from the same polychromatic source incident on a 20° VHF and 20° AVHF respectively. Note how only the green color is diffracted in (a) and a broader spectrum is seen in (b). (c) is a picture of the polychromatic noise (source+diffuser) diffracted by a 20° AVHF.

We believe that improvements can be made to further increase the spectral bandwidth of the AVHF system. Currently the AVHF filter is limited by the diffracted spectral bandwidth of the PD element in the 90° AVHF system and by the coupling efficiency between the PD and VHF in the 20° AVHF system.

4.2. SNR measurements

SNR measurements of the telescope arrangement, VHT, and AVHF configurations were made with the arrangements presented in Figs. 3(a)-(c). The telescope arrangement was used to measure

Optics EXPRESS

Table 1. VH System Spectral Bandwidths.[a]

Arrangement	Source	PD only	Holographic filter
VHF	200nm	-	20° = 8 nm 90° = 9 nm
AVHF	200nm	20° = 120nm 90° = 80nm	20° = 70nm 90° = 35nm

[a]Full-width half max spectral bandwidth measurements pertaining to the VHT and AVHF arrangements.

system SNR prior to the introduction of the VH systems. As discussed previously, the Rayleigh scattered noise was simulated by placing a 5° diffuser in front of the telescope arrangement.

SNR measurement results are summarized in Table 2. Using the telescopic arrangement alone (without any holographic elements) produced an SNR of 1.12 dB for the monochromatic signal/noise and an SNR of 2.12 dB for the polychromatic signal/noise. Concerning the monochromatic source/noise: the VHT arrangement, where a single VHF element is utilized, produced an SNR of 23.08 dB with the 20° VHF and SNR of 24.59 dB with the 90° VHF. Here the VHT system outperformed the AVHF which had an 11.4 dB and 16.04 dB for the 20° and 90° configuration respectively. These results were expected as the VHF was designed to perform optimally in this particular configuration where it was expected that the addition of the PD in the AVHF system would reduce the SNR due to a decrease in overall diffraction efficiency. Notably, the VHT configuration proves to be extremely useful for free space telecommunications, where a monochromatic laser signal is used. Concerning the monochromatic source/noise, which is expected to be used in the detection of satellites or space debris: the VHT system produced an SNR of 6.36 dB for a 20° VHF and SNR of 6.27 dB for a 90° VHF. Here, the AVHF outperformed the VHT system with SNR values of 8.54 dB and 9.73 dB for the 20° and 90° configurations respectively.

Table 2. Signal to Noise Measurements from VHT and AVHF Systems.[a]

Arrangement	Monochromatic Source and Noise SNR	Polychromatic Source and Noise SNR	System Spectral Bandwidth
Telescope	1.12 dB	2.12 dB	200nm
VHT	20° = 23.08 dB	20° = 6.36 dB	8 nm
	90° = 24.59 dB	90° = 6.27 dB	9 nm
AVHF	20° = 11.40 dB	20° = 8.54 dB	70 nm
	90° = 16.04 dB	90° = 9.73 dB	35 nm

[a]SNR measurements pertaining to a convention telescope arrangement, the VHT arrangement shaded in gray, the AVHF arrangement for both the monochromatic signal/noise and polychromatic signal/noise sources. Both the VHT and AVHF arrangements were tested using VH systems recorded at 20° and 90°.

To summarize, the reduction in SNR between monochromatic and polychromatic is expected in VH systems due to the wavelength selectivity giving rise to proportionally larger signal rejection. However, the AVHF system operates at a larger spectral bandwidth, which increases the diffraction efficiency of multiple wavelengths, leading to a proportionally smaller signal rejection when moving from a monochromatic source to a polychromatic source when compared to the VHT.

Optics EXPRESS

5. Conclusion

In this manuscript we have introduced the Advanced Volume Hologram Filtering (AVHF) system with aims at increasing the imaging spectral bandwidth whilst maintaining or increasing the retrievable SNR. The AVHF composed of two coupled holographic elements, a thin-volume hologram that acts as a pre-disperser (PD) and a thick-volume hologram (VHF), has demonstrated the potential to increases both the retrievable SNR and spectral bandwidth of imaged polychromatic sources when compared to state-of-the-art volume holographic filtering approaches. The current iteration of the AVHF system has a ~70nm spectral bandwidth and an SNR improvement of 7.61 dB (9.73 - 2.12 dB) when compared to a ~9nm bandwidth and 4.15 dB (6.27 – 2.12 dB) VHF alone.

Several improvements to the current AVHF design can be made to deploy the system in laboratory or real world imaging scenarios. Improving the diffraction efficiency of the thick PQ-doped PMMA VH as well as polishing of PQ-doped PMMA surfaces would allow for range based wavefront selectivity was well as improve over all image quality. With these potential improvements in mind we believe that that the AVHF could find applications in medical imaging and astronomy; where, microscopy, satellite detection, and free-space communication form some of the systems that would greatly benefit from the implementation of this technology.

Funding. U.S. Naval Research Laboratory.

Acknowledgments. The authors would like to thank the Naval Research Laboratory, Remote Sensing Division, Radio, Infrared and Optical Sensors Branch, and Applied Technology Associates, Washington Operations, for sponsoring this research.

Disclosures. The authors declare no conflicts of interest.

References

1. E. W. Rork, S. S. Lin, and A. J. Yakutis, "Ground-based electro-optical detection of artificial satellites in daylight from reflected sunlight," MIT Lincoln Laboratory Project Report ETS-63, (1982).
2. S. G. Garanin, I. V. Zhukov, L. I. Zykov, A. N. Klimov, A. V. Kopalkin, S. L. Openov, S. P. Smyshlyaev, and A. Yu. Syundyukov, "Daytime Observation of Low-brightness Stars (8m–10m) and Space Objects with a Video Camera Having Image Summation," J. Opt. Technol. **87**(7), 422 (2020).
3. J. Hughes, "Sky brightness as a function of altitude," Appl. Opt. **3**(10), 1135–1138 (1964).
4. G. V. Rozenberg, *Twilight a Study in Atmospheric Optics*. (Plenum, New York, 1966).
5. A. Hanel, P. Posch, S. J. Ribas, M. Aube, D. Duriscoe, A. Jechow, Z. Kollath, D. E. Lolkema, C. Moore, N. Schmidt, H. Spoelstra, G. Wuchterl, and C. C. M. Kyba, "Measuring Night Sky Brightness: Methods and Challenges," J. Quant. Spectrosc. Radiat. Transfer **205**, 278–290 (2018).
6. N. Jing, C. Li, and P. Zhong, "Ground-based optical detection of low-dynamic vehicles in near-space," Opt. Eng. **56**(1), 014107 (2017).
7. D. E. Chesser, D. Vunck, T. Born, W. Axelson, K. Rehder, and R. S. Medrano, "NIR daylight acquisition sensor improves mission capabilities," Proc. SPIE **5082**, 1–12 (2003).
8. S. G. Garanin, L. I. Zykov, A. N. Klimov, S. M. Kulikov, S. P. Smyshlyaev, V. V. Stepanov, and A. Yu. Syundyukov, "Daytime Observation of Low-brightness Stars (7m-8m) from Level Terrain," J. Opt. Technol. **84**(12), 816–821 (2017).
9. K. Jim, R. Wolfshagen, B. Gibson, E. Pier, K. Hodapp, and P. Onaka, "The HANDS-IONS Daytime Camera for GEO Satellite Characterization," *AMOS Conference Technical Proceedings*, (2011).
10. K. T. C. Jim, R. C. Wolfshagen, E. A. Pier, B. N. Gibson, D. Kokubun, and R. L. Cognion, "Daytime GEO Satellite Characterization with the HANDS-IONS Camera," *AISS Space 2012 Conference and Exposition*, Pasadena CA, (2012).
11. G. Thomas, R. Cobb, S. Fiorino, and M. Hawks, "SNR modeling for ground-based daytime imaging of GEO-satellites in the SWIR," *IEEE Aerospace Conference*, (2019).
12. A. Sinha and G. Barbastathis, "Volume Holographic Telescope," Opt. Lett. **27**(19), 1690–1692 (2002).
13. M. Fouchier, M. Zerrad, M. Lequime, and C. Amra, "Wide-range wavelength and angle resolved light scattering measurement setup," Opt. Lett. **45**(9), 2506–2509 (2020).
14. K. Bang, C. Jang, and B. Lee, "Compact Noise-filtering Volume Gratings for Holographic Displays," Opt. Lett. **44**(9), 2133–2136 (2019).
15. H. Gao, J. M. Watson, J. S. Stuart, and G. Barbastathis, "Design of volume hologram filters for suppression of daytime sky brightness in artificial satellite detection," Opt. Express **21**(5), 6448–6458 (2013).
16. Z. Chen, H. Gao, and G. Barbastathis, "Background suppression in long-distance imaging using volume hologram filters," Opt. Express **22**(25), 31123–31130 (2014).

Optics EXPRESS

17. Y. Luo, S. B. Oh, and G. George, "Wavelength-coded Multifocal Microscopy," Opt. Lett. **35**(5), 781–783 (2010).
18. I. D. Howlett, W. Han, P. Rice, J. K. Barton, and R. K. Kostuk, "Wavelength-coded Volume Holographic Imaging Endoscope for Multidepth Imaging," J. Biomed. Opt. **22**(10), 1 (2017).
19. K. Y. Hsu, S. H. Lin, Y. Hsiao, and W. T. Whang, "Experimental Characterization of Phenanthrenequinone-doped Poly(methyl Methacrylate) Photopolymer for Volume Holographic Storage," Opt. Eng. **42**(5), 1390–1396 (2003).
20. L. Yuan, P. J. Gelsinger, J. K. Barton, G. Barbastathis, and R. K. Kostuk, "Optimization of Multiplexed Holographic Gratings in PQ-PMMA for Spectral-spatial Imaging Filters," Opt. Lett. **33**(6), 566–568 (2008).
21. W. R. Klein and B. D. Cook, "Unified approach to ultrasonic light diffraction," IEEE Trans. Sonics Ultrason. **14**(3), 123–134 (1967).
22. A. Sinha, W. Sun, T. Shih, and G. Barbastathis, "Volume Holographic Imaging in Transmission Geometry," Appl. Opt. **43**(7), 1533–1551 (2004).
23. H. Kogelnik, "Coupled Wave Theory for Thick Hologram Gratings," The Bell Syst. Tech. J. **48**(9), 2909–2947 (1969).
24. G. Barbastathis, M. Balberg, and D. J. Brady, "Confocal Microscopy with a Volume Holographic Filter," Opt. Lett. **24**(12), 811–813 (1999).
25. I. D. Howlett, W. Han, M. Gordon, P. Rice, J. K. Barton, and R. K. Kostuk, "Volume Holographic Imaging Endoscopic Design and Construction Techniques," J. Biomed. Opt. **22**(5), 056010 (2017).
26. G. V. Orsinger, J. M. Watson, M. Gordon, A. C. Nymeyer, E. E. De Leon, J. W. Brownlee, K. D. Hatch, S. K. Chambers, J. K. Barton, R. K. Kostuk, and M. Romanowski, "Simultaneous Multiplane Imaging of Human Ovarian Cancer by Volume Holographic Imaging," J. Biomed. Opt. **19**(3), 036020 (2014).
27. G. J. Steckman, I. Solomatine, G. Zhou, and D. Psaltis, "Characterization of phenanthrenequinone-doped poly(methyl methacrylate) for holographic memory," Opt. Lett. **23**(16), 1310–1312 (1998).
28. V. N. Borisov and A. V. Veniaminov, "Angular Selectivity of Amplitude-Phase Holographic Gratings in Polymer Material with Phenanthrenequinone," Opt. Spectrosc. **124**(6), 901–907 (2018).
29. Y. Qi, E. Tolstik, H. Li, J. Guo, M. R. Gleeson, V. Matusevich, R. Kowarschik, and J. T. Sheridan, "Study of PQ/PMMA Photopolymer. Part 2: Experimental Results," J. Opt. Soc. Am. B **30**(12), 3308–3315 (2013).
30. V. N. Borisov and A. V. Veniaminov, "Determination of Refractive Index and Absorbance Modulation Amplitudes from Angular Selectivity of Holograms in Polymer Material with Phenanthrenequinone," Proc. SPIE **9545**, 954513 (2015).